Dynamics and Controls of a Generalized Frequency Domain Model Flexible Rotating Spacecraft

Tarek A. Elgohary*, James D. Turner† and John L. Junkins ‡

Modeling a flexible rotating spacecraft as a distributed parameters system of a rigid hub attached to a flexible appendage is very common. When considering large angle maneuvers the same model applies to flexible robotic manipulators by adding a tip mass at the end of the flexible appendage to account for the payload. Following Euler-Bernoulli beam theory the dynamics for both no tip mass and tip mass models are derived. A Generalized State Space (GSS) system is constructed in the frequency domain to completely solve for the input-output transfer functions of the models. The analytical solution of the GSS is obtained and compared against the classical assumed modes method. The frequency response of the system is then used in a classical control problem where a Lyapunov stable controller is derived and tested for gain selection. The assumed modes method is used to obtain the time response of the system to verify the gain selections and draw connections between the frequency and the time domains. The GSS approach provides a powerful tool to test various control schemes in the frequency domain and a validation platform for existing numerical methods utilized to solve distributed parameters models.

I. Introduction

A maneuvering flexible spacecraft is often modeled as coupled rigid hub, flexible beam-like structures. Two widely used models describing such systems are shown in Figure 1 and Figure 2. Figure 1 shows a model with a free end (no tip mass model), whereas Figure 2 is for a model with an attached mass at the end of the beam (tip mass model). Such models are described by coupled systems of Integro-Partial Differential Equations (IPDEs).[1–7] Solutions techniques presented in these works are mainly numerical applying finite elements methods and/or the assumed modes techniques. Numerical solutions in general are approximate and the accuracy is a function of the number of elements/modes chosen which can impose a high computational cost as the need arises for more accurate results. As a natural extension for such techniques the control problem is addressed in several works for optimality and/or robustness.[6,8–12] Analytical transfer functions for both models, no tip mas and tip mass, have been previously developed.[13–15] The transfer functions are used to analyze the system frequency response and numerical results are compared and verified against the assumed modes solution.

The control problem of a single axis rotating flexible spacecraft is addressed extensively utilizing several controls and modeling schemes. The optimal control problem of a rotating hub with symmetric four flexible appendages is presented as a numerical example.[16] An admissible function that meets both physical and geometrical boundary conditions is chosen. The effectiveness of the minimization rely on the number of modes retained in the series of the chosen admissible function. Finite elements techniques besides the assumed modes approach are used to solve a similar problem.[6] The natural frequencies of the system are calculated and the two methods are compared in terms of accuracy and the required number of elements/modes. Several other flexible structures examples are similarly addressed.[8] The optimal control problem is again addressed for various control schemes and penalty functions including free final time, free final angle and

*Graduate Research Assistant, Texas A&M University, Aerospace Engineering Department, 701 H.R. Bright Building, 3141 TAMU, College Station, Texas 77843-3141, AIAA Student Member.

†Research Professor, Texas A&M University, Aerospace Engineering Department, 745H H.R. Bright Building, 3141 TAMU, College Station, Texas 77843-3141.

‡Distinguished Professor, Texas A&M University, Aerospace Engineering Department, 722B H.R. Bright Building, 3141 TAMU, College Station, Texas 77843-3141.

control rate penalty methods. Large angle maneuvers for a flexible spacecraft are addressed for a hub-four flexible appendages model.[9] Two-point boundary value problems and kinematic nonlinearities are also addressed.[10] In a more recent work[17] the adaptive control problem is addressed for a similar rigid hub flexible appendage model. The proposed control scheme is independent of the truncation generated from the flexible modes admissible function because no series approximations are introduced. Several other works address similar problems with emphasis on optimality,[11,12,18–21] and/or robustness.[11,12] A comprehensive literature survey,[22] covers the modeling and control of flexible appendage in the controls community.

In this work the existence of the exact transfer functions[13–15] for both models is utilized in developing frequency domain control schemes for the spacecraft. The frequency response developed is used to obtain the gains required to implement a the controller that would drive the system from its initial state to a target state.

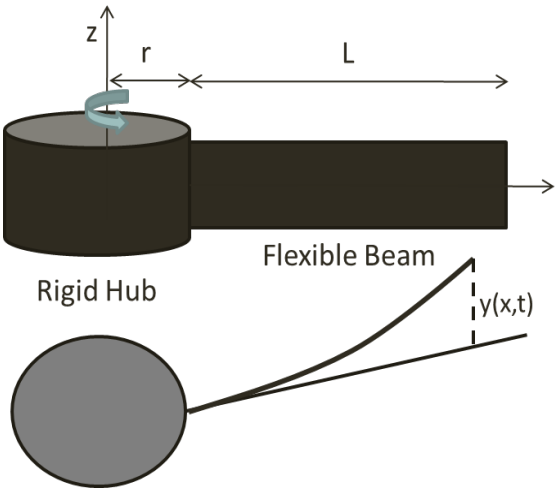

Figure 1. Hub-Beam Model

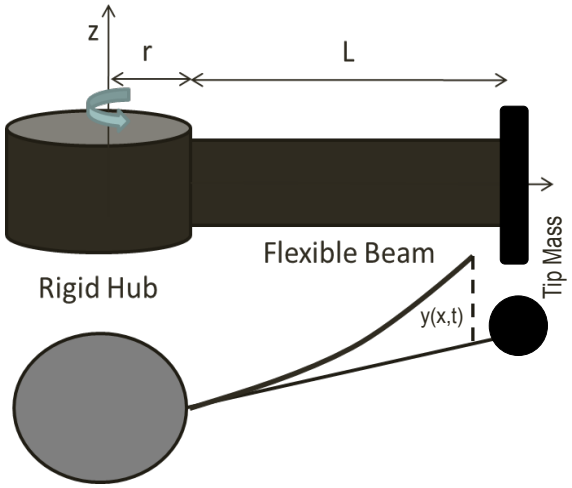

Figure 2. Hub-Beam-Tip Mass Model

II. The Generalized State Space Model

The more general hub-beam-tip mass model equations are derived knowing that by setting the tip mass and the tip inertia to 0 the hub-beam model can be obtained. The inertial position and velocity of a point on the flexible appendage is given by,

$$\mathbf{p} = (x+r)\,\hat{\mathbf{b_1}} + y\hat{\mathbf{b_2}} \tag{1}$$

$$\mathbf{v} = \dot{y}\hat{\mathbf{b_2}} + \dot{\theta}\hat{\mathbf{b_3}} \times \left[(x+r)\,\hat{\mathbf{b_1}} + y\hat{\mathbf{b_2}}\right] \tag{2}$$

where, r is the rotating hub radius, L the length of the flexible appendage, $x \in [0, L]$ the position on the flexible appendage and y the transverse deflection of the flexible appendage. Neglecting the $y\dot{\theta}$ term in the velocity, the kinetic energy and the potential energy for the tip mass model are expressed as,[6]

$$\begin{aligned} T &= T_{\text{hub}} + T_{\text{appendage}} + T_{\text{tip}} \\ T &= \frac{1}{2}I_{\text{hub}}\dot{\theta}^2 + \frac{1}{2}\int_0^L \rho\left(\dot{y} + (x+r)\dot{\theta}\right)^2 \mathrm{d}x + \frac{1}{2}m_{\text{tip}}\left((r+L)\dot{\theta} + \dot{y}(L)\right)^2 + \frac{1}{2}I_{\text{tip}}\left(\dot{\theta} + \dot{y}'(L)\right)^2 \end{aligned} \tag{3}$$

$$V = \frac{1}{2}\int_0^L EI\left(y''\right)^2 \mathrm{d}x \tag{4}$$

Applying Hamilton's extended principle the system equations of motion and boundary conditions can be expressed as,

$$\begin{aligned} I_{\text{hub}}\ddot{\theta} + \int_0^L \rho(x+r)\left(\ddot{y} + (x+r)\ddot{\theta}\right)\mathrm{d}x + m_{\text{tip}}(L+r)\left((L+r)\ddot{\theta} + \ddot{y}(L)\right) + I_{\text{tip}}\left(\ddot{\theta} + \ddot{y}'(L)\right) &= u \\ \rho\left(\ddot{y} + (x+r)\ddot{\theta}\right) + EIy^{IV} &= 0 \end{aligned} \tag{5}$$

$$
\begin{aligned}
&\text{at } x = 0 : y = 0, \quad y' = 0 \\
&\text{at } x = L : EI\frac{\partial^3 y}{\partial x^3}\bigg|_L = m_{\text{tip}}\left((L+r)\ddot{\theta} + \ddot{y}(L)\right), \quad EI\frac{\partial^2 y}{\partial x^2}\bigg|_L = -I_{\text{tip}}\left(\ddot{\theta} + \ddot{y}'(L)\right)
\end{aligned} \tag{6}
$$

By setting $m_{\text{tip}} = I_{\text{tip}} = 0$ the no tip mass model, Figure 1, dynamics and boundary conditions are obtained as,

$$
\begin{aligned}
I_{\text{hub}}\ddot{\theta} + \int_0^L \rho(x+r)\left(\ddot{y} + (x+r)\ddot{\theta}\right)\,\mathrm{d}x &= u \\
\rho\left(\ddot{y} + (x+r)\ddot{\theta}\right) + EIy^{IV} &= 0
\end{aligned} \tag{7}
$$

$$
\begin{aligned}
&\text{at } x = 0 : y = 0, \quad y' = 0 \\
&\text{at } x = L : EI\frac{\partial^3 y}{\partial x^3}\bigg|_L = 0, \quad EI\frac{\partial^2 y}{\partial x^2}\bigg|_L = 0
\end{aligned} \tag{8}
$$

A generalized state space (GSS) model is developed by taking the Laplace transform, Eq. (9), for Eq. (5) and performing integration by parts to remove the spatial dependency from the integral. Detailed steps for the GSS derivation is presented in previous works.[14,15]

$$
F(s) = \int_0^\infty e^{-st} f(t)\,\mathrm{d}t \tag{9}
$$

$$
\begin{aligned}
z_1 &= \iint \bar{y}\,\mathrm{d}x\,\mathrm{d}x' & z_1' &= z_2 \\
z_2 &= \int \bar{y}\,\mathrm{d}x & z_2' &= z_3 \\
z_3 &= \bar{y} & z_3' &= z_4 \\
z_4 &= \bar{y}' & z_4' &= z_5 \\
z_5 &= \bar{y}'' & z_5' &= z_6 \\
z_6 &= \bar{y}''' & z_6' &= -\beta\left(z_3 + (r+x)\bar{\theta}\right)
\end{aligned}
\qquad \text{where, } \beta \equiv \frac{s^2\rho}{EI} \tag{10}
$$

The generalized state space model system of equations is solved by first developing the homogeneous and the forced solutions for the linear state space model in Eq. (10),

$$
\{Z(x)\} = \underbrace{\exp[Ax]\,\{Z(0)\}}_{Z_H} + \underbrace{\int_0^x \exp\left[A(x-\tau)\right]\{b(\tau)\}\,\mathrm{d}\tau}_{Z_F} \tag{11}
$$

where the homogeneous solution Z_H is given by,

$$
\{Z_H\} = \begin{Bmatrix}
(1-f)z_5/\beta - (\beta x + f''')z_6/\beta^2 \\
-f'z_5/\beta + (1-f)z_6/\beta \\
-f''z_5/\beta - f'z_6/\beta \\
-f'''z_5/\beta - f''z_6/\beta \\
fz_5 - f'''z_6/\beta \\
f'z_5 + fz_6
\end{Bmatrix} \tag{12}
$$

and the forced part is evaluated from,

$$
\{Z_F\} = \int_0^x \exp\left[A(x-\tau)\right]\{b(\tau)\}\,\mathrm{d}\tau = -\beta\bar{\theta}\int_0^x (r+\tau)\begin{Bmatrix}
\left(\beta(x-\tau) + f'''(x-\tau)\right)/\beta^2 \\
\left(1 - f(x-\tau)\right)/\beta \\
-f'(x-\tau)/\beta \\
-f''(x-\tau)/\beta \\
-f'''(x-\tau)/\beta \\
f(x-\tau)
\end{Bmatrix}\mathrm{d}\tau \tag{13}
$$

The funtion f that represents the elements of the solution is derived from the matrix exponential solution of the flexible appendage sub-problem and is given by,[14,15]

$$f(x) = \cos\left(\frac{\beta^{1/4}x}{\sqrt{2}}\right)\cosh\left(\frac{\beta^{1/4}x}{\sqrt{2}}\right) \tag{14}$$

It is observed that the function f represents the real part of the complex function

$$f = Re\left\{\cos(\sigma x)\right\}, \quad \text{where, } \sigma \equiv \sqrt{i\sqrt{\beta}} \tag{15}$$

The homogeneous solution in Eq. (12) can now be represented as,

$$\{Z_H\} = \begin{Bmatrix} (1-\cos(\sigma x))z_5/\beta + (\beta x + \sigma^3\sin(\sigma x))z_6/\beta^2 \\ \sigma\sin(\sigma x)z_5/\beta + (1-\cos(\sigma x))z_6/\beta \\ \sigma^2\cos(\sigma x)z_5/\beta + \sigma\sin(\sigma x)z_6/\beta \\ -\sigma^3\sin(\sigma x)z_5/\beta + \sigma^2\cos(\sigma x)z_6/\beta \\ \cos(\sigma x)z_5 - \sigma^3\sin(\sigma x)z_6/\beta \\ -\sigma\sin(\sigma x)z_5 + \cos(\sigma x)z_6 \end{Bmatrix} \tag{16}$$

Similarly, the forced part of the solution, Eq. (13), is obtained as,

$$\{Z_F\} = \begin{Bmatrix} \frac{1}{6\beta}\left(-3\beta r x^2 - \beta x^3 + 6\sigma^2 r\cos(\sigma x) + 6\sigma\sin(\sigma x) - 6\sigma^2 r - 6\sigma^2 x\right)\bar{\theta} \\ \frac{1}{2\sigma^2}\left(-2\sigma^2 r x - \sigma^2 x^2 + 2\sigma r\sin(\sigma x) - 2\cos(\sigma x) + 2\right)\bar{\theta} \\ \frac{1}{\sigma}\left(\sigma r\cos(\sigma x) + \sin(\sigma x) - \sigma r - \sigma x\right)\bar{\theta} \\ \left(-\sigma r\sin(\sigma x) + \cos(\sigma x) - 1\right)\bar{\theta} \\ -\sigma\left(\sigma r\cos(\sigma x) + \sin(\sigma x) - \sigma r - \sigma x\right)\bar{\theta} \\ -\frac{1}{\sigma^2}\left(\beta\left(\sigma r\sin(\sigma x) - \cos(\sigma x) + 1\right)\right)\bar{\theta} \end{Bmatrix} = \begin{Bmatrix} I_1(x) \\ I_1(x) \\ I_3(x) \\ I_4(x) \\ I_5(x) \\ I_6(x) \end{Bmatrix}\bar{\theta} \tag{17}$$

Equations (16) and (17) are combined to produce the full GSS solution as a function of z_5 and z_6.

$$\{Z(x)\} = \begin{Bmatrix} (1-\cos(\sigma x))z_5/\beta + (\beta x + \sigma^3\sin(\sigma x))z_6/\beta^2 + I_1(x)\bar{\theta} \\ \sigma\sin(\sigma x)z_5/\beta + (1-\cos(\sigma x))z_6/\beta + I_2(x)\bar{\theta} \\ \sigma^2\cos(\sigma x)z_5/\beta + \sigma\sin(\sigma x)z_6/\beta + I_3(x)\bar{\theta} \\ -\sigma^3\sin(\sigma x)z_5/\beta + \sigma^2\cos(\sigma x)z_6/\beta + I_4(x)\bar{\theta} \\ \cos(\sigma x)z_5 - \sigma^3\sin(\sigma x)z_6/\beta + I_5(x)\bar{\theta} \\ -\sigma\sin(\sigma x)z_5 + \cos(\sigma x)z_6 + I_6(x)\bar{\theta} \end{Bmatrix} \tag{18}$$

The solution of the GSS model in Eq. (18) is obviously invariant to the model and its related boundary conditions. By applying the specific model boundary conditions and solving for the state variables, z_5, z_6, the solution is complete in terms of the known system parameters. This makes the GSS solution capable of handling a wide range of distributed parameters problems as the need to apply the model specific boundary conditions arises at the last step of the solution. Applying the model dependent boundary conditions, Eq. (19) for the no tip mass model shown in Figure 1, z_5, z_6 are completely solved in Eq. (20)

$$\begin{aligned} &\text{at } x = 0 : \{Z\} = \begin{bmatrix} 0 & 0 & 0 & 0 & z_5 & z_6 \end{bmatrix}^{\mathrm{T}} \\ &\text{at } x = L : z_5(L) = 0, \quad z_6(L) = 0 \\ &\text{where, } \alpha \equiv \frac{s^2 I_{\text{tip}}}{EI} \quad \text{and} \quad \gamma \equiv \frac{s^2 m_{\text{tip}}}{EI} \end{aligned} \tag{19}$$

$$\begin{Bmatrix} z_5 \\ z_6 \end{Bmatrix} = \frac{1}{\sigma^4\sin(\sigma L)/\beta - \cos(\sigma L)^2}\begin{bmatrix} \cos(\sigma L) & \sigma^3\sin(\sigma L)/\beta \\ \sigma\sin(\sigma L) & \cos(\sigma L) \end{bmatrix}\begin{Bmatrix} I_5(L) \\ I_6(L) \end{Bmatrix}\bar{\theta} \tag{20}$$

For the model with tip mass shown in Figure 2, the boundary conditions are,

$$\begin{aligned}
&\text{at } x = 0 : \{Z\} = \begin{bmatrix} 0 & 0 & 0 & 0 & z_5 & z_6 \end{bmatrix}^{\mathrm{T}} \\
&\text{at } x = L : z_5(L) = -\alpha \left[z_4(L) + \bar{\theta} \right], \quad z_6(L) = \gamma \left[z_3(L) + (r+L)\bar{\theta} \right] \\
&\text{where, } \alpha \equiv \frac{s^2 I_{\text{tip}}}{EI} \quad \text{and} \quad \gamma \equiv \frac{s^2 m_{\text{tip}}}{EI}
\end{aligned} \tag{21}$$

and z_5, z_6 are obtained from,

$$\begin{aligned}
\begin{Bmatrix} z_5 \\ z_6 \end{Bmatrix} &= \frac{1}{\sigma^4 \sin(\sigma L)^2/\beta - \cos(\sigma L)^2} \begin{bmatrix} -\alpha\cos(\sigma L) & \gamma\sigma^3 \sin(\sigma L)/\beta \\ -\alpha\sigma \sin(\sigma L) & \gamma \cos(\sigma L) \end{bmatrix} \begin{Bmatrix} z_4(L) \\ z_3(L) \end{Bmatrix} \\
&\quad + \begin{bmatrix} \sigma^3 \left(\gamma(r+L) - I_6(L)\right)/\beta & (-\alpha - I_5(L)) \\ \sigma \left(-\alpha - I_5(L)\right) & \gamma(r+L) - I_6(L) \end{bmatrix} \begin{Bmatrix} \sin(\sigma L) \\ \cos(\sigma L) \end{Bmatrix} \bar{\theta} \\
\begin{Bmatrix} z_4(L) \\ z_3(L) \end{Bmatrix} &= \frac{1}{\beta} \begin{bmatrix} -\sigma^3 \sin(\sigma L) & \sigma^2 \cos(\sigma L) \\ \sigma^2 \cos(\sigma L) & \sigma \sin(\sigma L) \end{bmatrix} \begin{Bmatrix} z_5 \\ z_6 \end{Bmatrix} + \begin{Bmatrix} I_4(L) \\ I_3(L) \end{Bmatrix} \bar{\theta}
\end{aligned} \tag{22}$$

Detailed derivations of solutions in Eq. (20) and Eq. (22) are presented in previous works.[14,15] The expressions obtained can then be expressed in the general form,

$$\{Z(x)\} = \begin{Bmatrix} g_1(x) \\ g_2(x) \\ g_3(x) \\ g_4(x) \\ g_5(x) \\ g_6(x) \end{Bmatrix} \bar{\theta} \tag{23}$$

For the no tip mass model, from Eq. (7) the rotation angle of the rigid hub is associated with the input torque by,

$$\begin{aligned}
&s^2 \left[J_1 + \rho \left((r+x) g_2(x) - g_1(x) \right) \right] \bar{\theta} = \bar{u} \\
&\bar{\theta} = \frac{\bar{u}}{s^2 \left[J_1 + \rho \left((r+x) g_2(x) - g_1(x) \right) \right]}
\end{aligned} \tag{24}$$

and from the GSS model, Eq. (10), the beam deformation is given by,

$$\bar{y} = g_3(x)\bar{\theta} = \frac{g_3(x)}{s^2 \left[J_1 + \rho \left((r+x) g_2(x) - g_1(x) \right) \right]} \bar{u} \tag{25}$$

where, $J_1 \equiv I_{\text{hub}} + \int_0^L \rho (r+x)^2 \, \mathrm{d}x$ is the total inertia. Similarly for the tip mass model, the beam deformation $\bar{y}$ is represented as a function of the input torque $\bar{u}$ as,

$$\begin{aligned}
&s^2 \left[J_2 + m_{\text{tip}}(r+L) g_3(L) + I_{\text{tip}} g_4(L) + \rho \left((r+x) g_2(x) - g_1(x) \right) \right] \bar{\theta} = \bar{u} \\
&\bar{\theta} = \frac{\bar{u}}{s^2 \left[J_2 + m_{\text{tip}}(r+L) g_3(L) + I_{\text{tip}} g_4(L) + \rho \left((r+x) g_2(x) - g_1(x) \right) \right]} \\
&\bar{y} = \frac{g_3(x)}{s^2 \left[J_2 + m_{\text{tip}}(r+L) g_3(L) + I_{\text{tip}} g_4(L) + \rho \left((r+x) g_2(x) - g_1(x) \right) \right]} \bar{u}
\end{aligned} \tag{26}$$

where the total inertia in that case is $J_2 \equiv I_{\text{hub}} + m_{\text{tip}}(r+L)^2 + I_{\text{tip}} + \int_0^L \rho (r+x)^2 dx$

III. Frequency Response Numerical Results

From Eq. (25) and Eq. (26), the transfer function of the no tip mass model, $G_1(s,x)$, and the tip mas model $G_2(s,x)$ are expressed as,

$$\begin{aligned} G_1(s,x) &= \frac{g_3(x)}{s^2\left[J_1 + \rho\left((r+x)g_2(x) - g_1(x)\right)\right]} \\ G_2(s,x) &= \frac{g_3(x)}{s^2\left[J_2 + m_{\text{tip}}(r+L)g_3(L) + I_{\text{tip}}g_4(L) + \rho\left((r+x)g_2(x) - g_1(x)\right)\right]} \end{aligned} \tag{27}$$

For the purpose of comparison the classical assumed modes solution[6] is utilized. The method assumes a decoupled spatial and time dependent beam response expressed with the series,

$$y(x,t) = \sum_{i=1}^{N} q_i(t)\phi_i(x) \tag{28}$$

The spatial function $\phi_i(x)$ describes the i-th spatial mode of the flexible structure and is designed to meet the physical and the geometrical boundary conditions of the beam. A widely used admissible function that satisfies the boundary conditions is,[6,10]

$$\begin{aligned} &\phi_i(x) = 1 - \frac{\cos(i\pi x)}{L} + \frac{1}{2}(-1)^{i+1}\left(\frac{i\pi x}{L}\right)^2 \\ &\text{where, } 0 \le x \le L \end{aligned} \tag{29}$$

Using Eq. (28) and Eq. (29) with Eq. (3) and Eq. (4) and following the Lagrangian approach,

$$\frac{d}{dt}\left(\frac{\partial T}{\partial \mathbf{x}}\right) - \frac{\partial T}{\partial \mathbf{x}} + \frac{\partial V}{\partial \mathbf{x}} = \mathbf{F} \tag{30}$$

the system of equations of motion for the tip mass model is represented in the matrix form,

$$\begin{bmatrix} J_2 & M_{\theta q}^{\mathrm{T}} \\ M_{\theta q} & M_{qq} \end{bmatrix} \ddot{\mathbf{x}} + \begin{bmatrix} 0 & 0 \\ 0 & K_{qq} \end{bmatrix} \mathbf{x} = \begin{Bmatrix} u \\ 0 \end{Bmatrix} \tag{31}$$

where the elements of the mass and the stiffness matrices are defined as,

$$\begin{aligned} J_2 &= I_{\text{hub}} + m_{\text{tip}}(r+L)^2 + I_{\text{tip}} + \int_0^L \rho(r+x)^2\,\mathrm{d}x \\ \left[M_{\theta q}\right]_i &= \rho\int_0^L (r+x)\phi_i(x)\,\mathrm{d}x + m_{\text{tip}}(r+L)\phi_i(L) + I_{\text{tip}}\phi_i'(L) \\ \left[K_{qq}\right]_{ij} &= \int_0^L \phi_i''(x)\phi_j''(x)\,\mathrm{d}x \end{aligned} \tag{32}$$

In order to obtain the no tip mass model equations, one can set $m_{\text{tip}} = I_{\text{tip}} = 0$ in Eq. (32) to obtain the mass and stiffness matrices elements for the model. A comparison between the frequency response of the analytical GSS and the numerical assumed modes method, assuming 10 modes, is presented in Figure 3 and Figure 4 for the no tip mass model at $x = 2$ ft. and $x = 4$ ft., respectively. The set of parameters values used in this comparison are extracted from a physical model[6] and are shown in Table 1. Similar results are obtained for the tip mass model and are shown in Figure 5 and Figure 6

IV. The Control Problem

Building on the analytical solution obtained for the more general tip mass model, the control problem is analyzed. To gain some insight on the system behavior, the unit step input Bode plots are generated at the midpoint of the appendage $x = 2$ ft. for both the responses of rigid body, $\bar{\theta}(j\omega)$, and the flexible appendage,

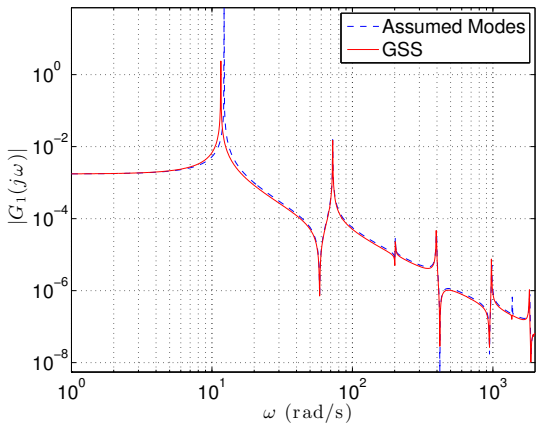

Figure 3. Frequency Response Comparison No Tip Mass Model at $x = 2$ ft

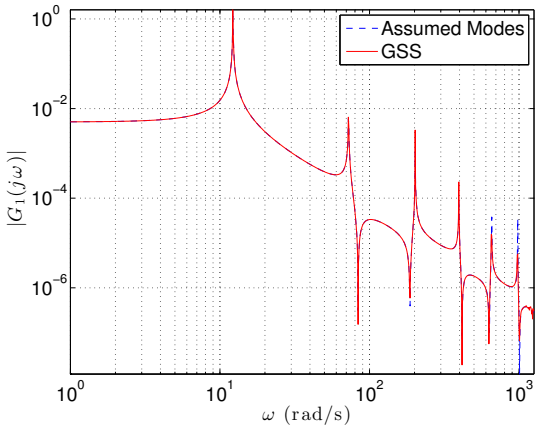

Figure 4. Frequency Response Comparison No Tip Mass Model at $x = 4$ ft

Table 1. System Parameters Values

Parameter	Value
I_{hub}	8 slug-ft^2
ρ	0.0271875 slug/ft
E	0.1584×10^{10} lb/ft^2
L	4 ft
r	1 ft
I	0.47095×10^{-7} ft^4
m	0.1569 slug
I_{tip}	0.0018 slug-ft^2

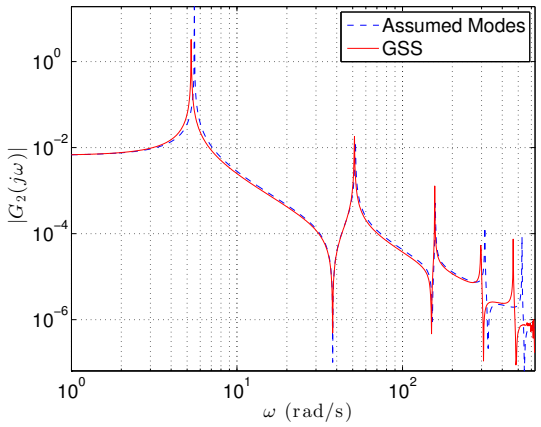

Figure 5. Frequency Response Comparison Tip Mass Model at $x = 2$ ft

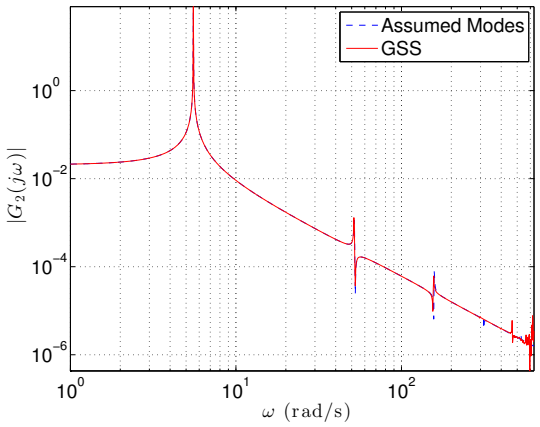

Figure 6. Frequency Response Comparison Tip Mass Model at $x = 4$ ft

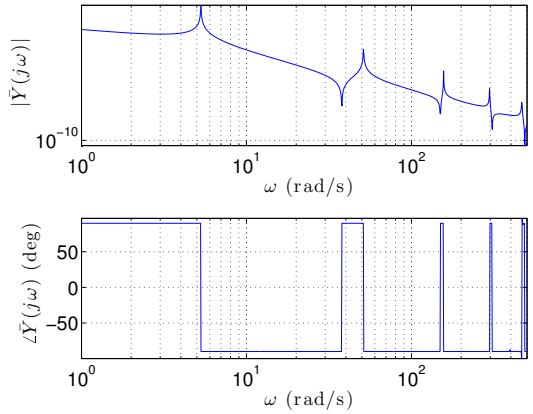

Figure 7. Bode Plot $\bar{Y}$ at $x = 2$ ft

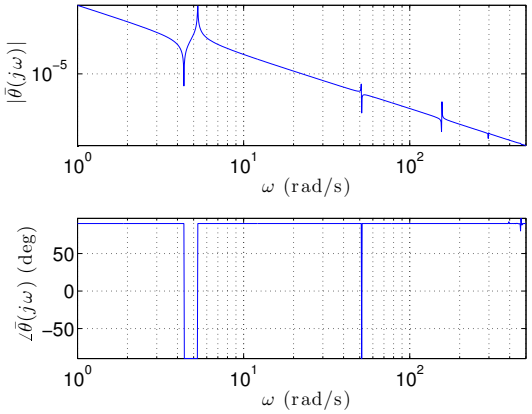

Figure 8. Bode Plot $\bar{\theta}$ at $x = 4$ ft

$\bar{y}(j\omega)$, Figure 7 and Figure 8 respectively. The resonant behavior of the system previously obtained from the GSS tranfer function, Eq. (27), is clearly present in this analysis with the phase angle shifting between $+90°$ and $-90°$ at those frequencies. For further insights, the assumed modes method is used to generate the model time response for a unit step input for $\theta(t)$, $\theta(t)$, Figure 9 and Figure 10, and for $y(x,t)$, $\dot{y}(x,t)$, Figure 11 and Figure 12. A case study is constructed for the more general tip mass model applying a Lyapunov stable controller.[6] First Eq. (5) is rewritten as,

$$\begin{aligned} &I_{\text{hub}}\ddot{\theta} = u + (M_0 - rS_0) \\ &-(M_0 - rS_0) = \int_0^L \rho(x+r)\left(\ddot{y} + (x+r)\ddot{\theta}\right)\,\mathrm{d}x + m_{\text{tip}}(L+r)\left((L+r)\ddot{\theta} + \ddot{y}(L)\right) \\ &\rho\left(\ddot{y} + (x+r)\ddot{\theta}\right) + EIy^{IV} = 0 \end{aligned} \tag{33}$$

where, (M_0, S_0) represent the bending moment and shear force at the root of the beam. The effect of the tip mass inertia is left out for simplification and can be considered as a disturbance error or as part of the model uncertainty the controller needs to overcome. The set of boundary conditions in Eq. (6) can then be simplified as,

$$\begin{aligned} &\text{at } x = 0 : y = 0, \quad y' = 0 \\ &\text{at } x = L : EI\frac{\partial^3 y}{\partial x^3}\bigg|_L = m_{\text{tip}}\left((L+r)\ddot{\theta} + \ddot{y}(L)\right), \quad EI\frac{\partial^2 y}{\partial x^2}\bigg|_L = 0 \end{aligned} \tag{34}$$

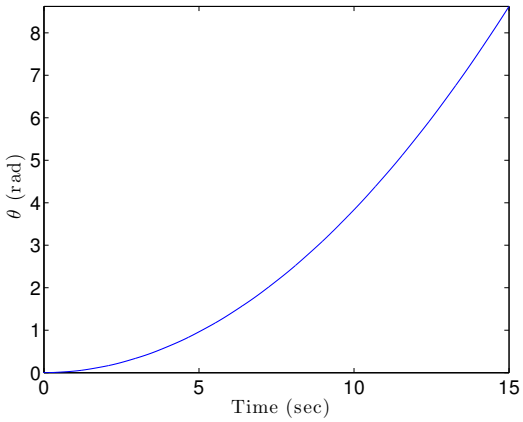

Figure 9. Step Input Response $\theta(t)$

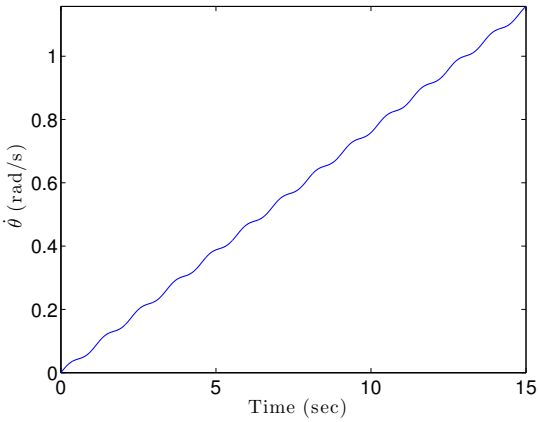

Figure 10. Step Input Response $\dot{\theta}(t)$

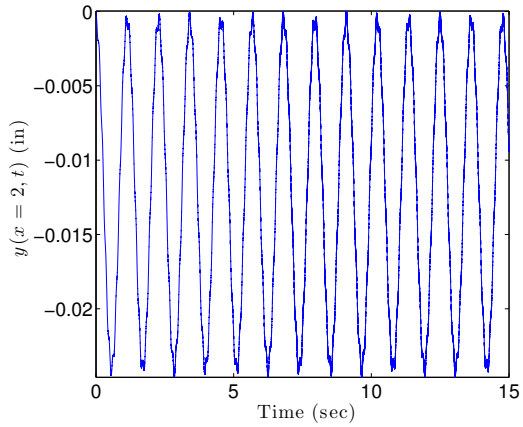

Figure 11. Step Input Response $y(x = 2, t)$

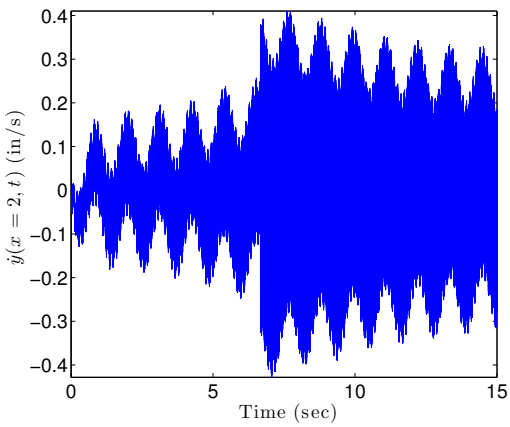

Figure 12. Step Input Response $\dot{y}(x = 2, t)$

We are interested in large angle maneuvers with a target final state given by,

$$\left[\theta, \dot{\theta}, y(x,t), \dot{y}(x,t)\right]_{\text{Target}} = [\theta_f, 0, 0, 0] \tag{35}$$

A weighted Lyapunov function is then given by,

$$\begin{aligned} 2V &= w_1 I_{\text{hub}} \dot{\theta}^2 + w_2 \left(\theta - \theta_f\right)^2 \\ &+ w_3 \left[\int_0^L \rho \left(\dot{y} + (x+r)\dot{\theta}\right)^2 \, \mathrm{d}x + m_{\text{tip}} \left((r+L)\dot{\theta} + \dot{y}(L)\right)^2 + \int_0^L EI \left(y''\right)^2 \, \mathrm{d}x\right] \end{aligned} \tag{36}$$

where an extra term that includes a penalty for the current state versus the target state, $(\theta - \theta_f)$ is added to achieve the required maneuver. By differentiating the Lyapunov function, Eq. (36) w.r.t. time and substituting the dynamics, Eq. (33), and the boundary conditions, Eq. (34), $\dot{V}$ can be expressed as,

$$\begin{aligned} \dot{V} &= w_1 u \dot{\theta} + w_2 \left(\theta - \theta_f\right) \dot{\theta} \\ &+ \left(w_3 - w_1\right) \left[\int_0^L \rho (x+r) \left(\ddot{y} + (x+r)\ddot{\theta}\right) \, \mathrm{d}x + m_{\text{tip}} (L+r) \left((L+r)\ddot{\theta} + \ddot{y}(L)\right)\right] \dot{\theta} \\ &= \left[w_1 u + w_2 \left(\theta - \theta_f\right) + \left(w_3 - w_1\right) \left(r S_0 - M_0\right)\right] \dot{\theta} \end{aligned} \tag{37}$$

In order to ensure stability, $\dot{V}$ should meet the condition $\dot{V} \leq 0$ and the control law is chosen as,

$$u = \frac{-1}{w_1} \left[w_2 \left(\theta - \theta_f\right) + \left(w_3 - w_1\right) \left(r S_0 - M_0\right) + w_4 \dot{\theta}\right] \tag{38}$$

By substituting Eq. (38) into Eq. (37), the negative semi-definite expression, $\dot{V} = -w_4 \dot{\theta}^2 \leq 0$ is obtained. In order to simplify the gain choices associated with the control law, Eq. (38) can be re-written as,

$$u = -\left[k_1 \left(\theta - \theta_f\right) + k_2 \left(r S_0 - M_0\right) + k_3 \dot{\theta}\right] \tag{39}$$

where, $k_1 \equiv \frac{w_2}{w_1} \geq 0$, $k_2 \equiv \frac{w_3 - w_1}{w_1} > -1$ and $k_3 \equiv \frac{w_4}{w_1} \geq 0$. The sign and value of k_2 will determine whether the beam vibration energy, $w_3 - w_1 > 0$, or the hub motion energy, $w_1 > w_3$ is dissipated. To investigate the frequency domain response applying the control law, the Laplace transformation of Eq. (39) is expressed as,

$$\bar{u} = -k_1 \left(\bar{\theta} - \frac{\theta_f}{s}\right) - k_2 \left(\rho s^2 \int_0^L (x+r) \left(\bar{y} + (x+r)\bar{\theta}\right) \, \mathrm{d}x + m_{\text{tip}} s^2 (L+r) \left((L+r)\bar{\theta} + \bar{y}(L)\right)\right) - k_3 s \bar{\theta} \tag{40}$$

Utilizing integration by parts the transformed control law is expressed in terms of the GSS state variables as,

$$\begin{aligned} \bar{u} = &\left[-k_1 - k_2 \rho s^2 \int_0^L (r+x)^2 \, \mathrm{d}x - k_2 m_{\text{tip}} s^2 (L+r)^2 - k_3 s\right] \bar{\theta} \\ &+ k_1 \frac{\theta_f}{s} - k_2 \rho s^2 \left((x+r) g_2(x) - g_1(x)\right) - k_2 m_{\text{tip}} s^2 (L+r) g_3(L) \end{aligned} \tag{41}$$

Substituting Eq. (41) into the transfer function, Eq. (26), and collecting variables produced the transfer function for the hub angle $\bar{\theta}$ as,

$$\begin{aligned} \bar{\theta} = &\left[k_1 \frac{\theta_f}{s} - k_2 \rho s^2 \left((x+r) g_2(x) - g_1(x)\right) - k_2 m_{\text{tip}} s^2 (L+r) g_3(L)\right] / \\ &s^2 \left[\frac{k_1}{s^2} + k_2 \rho \int_0^L (r+x)^2 \, \mathrm{d}x + k_2 m_{\text{tip}} (L+r)^2 + \frac{k_3}{s} + J_2 + m_{\text{tip}} (r+L) g_3(L) + I_{\text{tip}} g_4(L) + \rho \left((r+x) g_2(x) - g_1(x)\right)\right] \end{aligned} \tag{42}$$

The deformation transfer function can then be expressed in terms of $\bar{\theta}$ as,

$$\bar{y} = g_3(x) \bar{\theta} \tag{43}$$

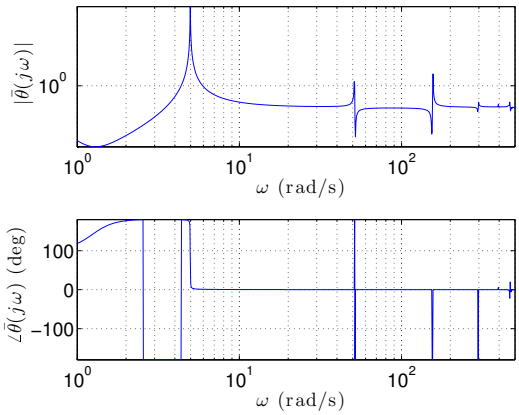

Figure 13. Bode Plot $\bar{\Theta}$, Unit Gains

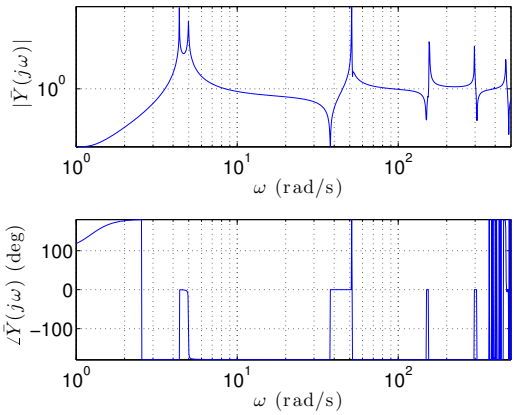

Figure 14. Bode Plot $\bar{Y}$ Unit Gains

After some trial and error the controller gains are adjusted to obtain the most stable response. To illustrate the effect of gain changes on the system frequency response the gains are first set to $k_1 = 1, k_2 = 1, k_3 = 1$. Figure 13 and Figure 14 show the Bode plots associated with the two transfer functions, Eq. (42) and Eq. (43), respectively, for unit gains. Clearly, the frequency response highlights potential system instability with order of magnitude gain amplifications and a $-180°$ phase angle. The gains are then adjusted to $k_1 = 12, k_2 = 0, k_3 = 16$. The Bode plots associated with the designed gains are shown in Figure 15 and Figure 16.

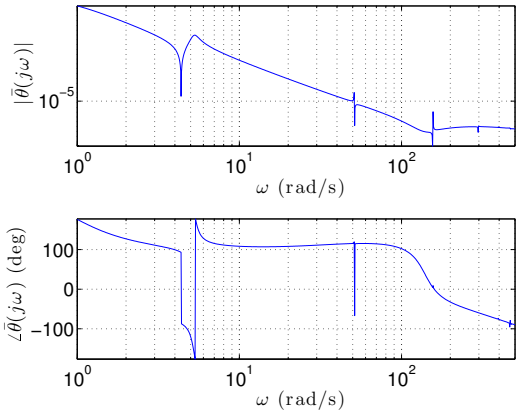

Figure 15. Bode Plot $\bar{\Theta}$, Designed Gains

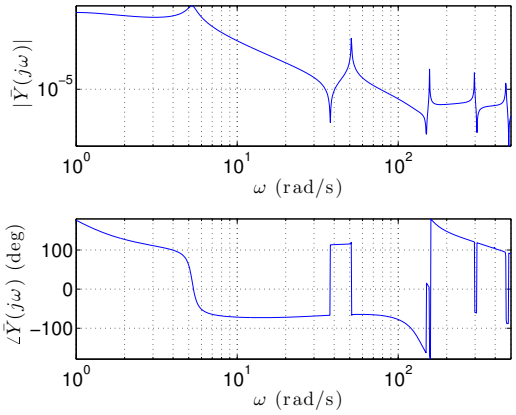

Figure 16. Bode Plot $\bar{Y}$ Designed Gains

With no significant lags or high amplitude amplification, the chosen set of parameters can be suitable for a controller to drive the rigid hub to its target final angle while mitigating the vibrations effect of the appendage. The time response plots for the system are shown for $\theta(t)$, $\dot{\theta}(t)$, in Figure 17 and Figure 18, and for $y(x = 2, t)$, $\dot{y}(x = 2, t)$ in Figure 19 and Figure 20.
The results show achieving the target state for θ and $\dot{\theta}$ whereas, $y(x, t)$ and $\dot{y}(x, t)$ still need more fine tuning. This can be achieved by several methods one of which is to construct a tracking problem with a smooth bang-bang controller.[6] Another approach is to apply notch compensation to mitigate the high frequency oscillations in the appendage. Several of those ideas can be implemented and tested with the fully solved frequency response of the system.

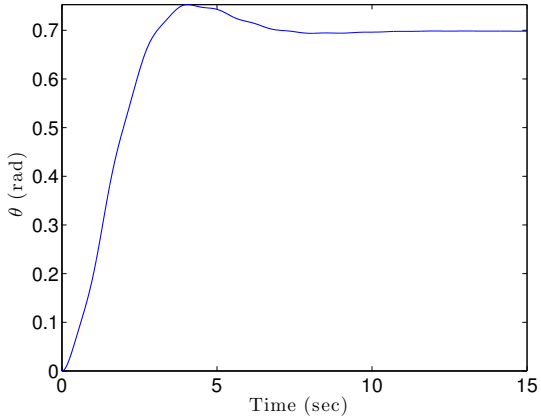

Figure 17. $\theta(t)$ **Designed Gains**

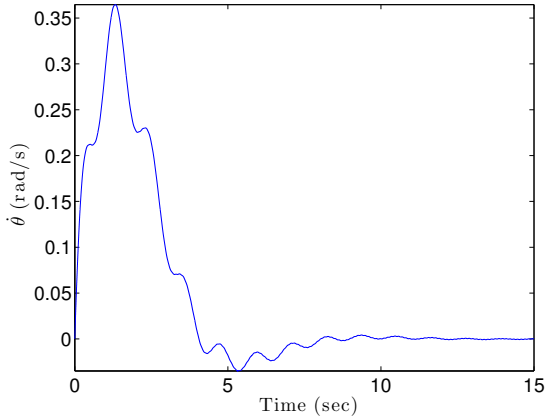

Figure 18. $\dot{\theta}(t)$ **Designed Gains**

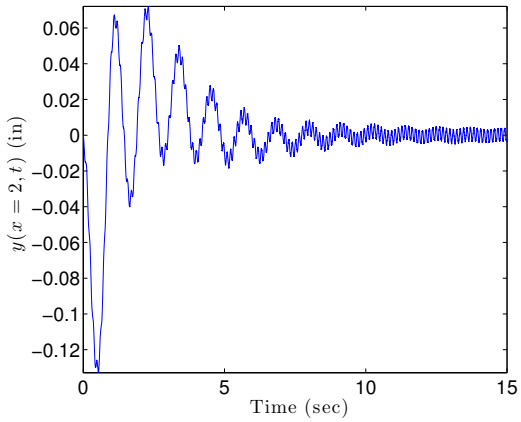

Figure 19. $y(x = 2, t)$ **Designed Gains**

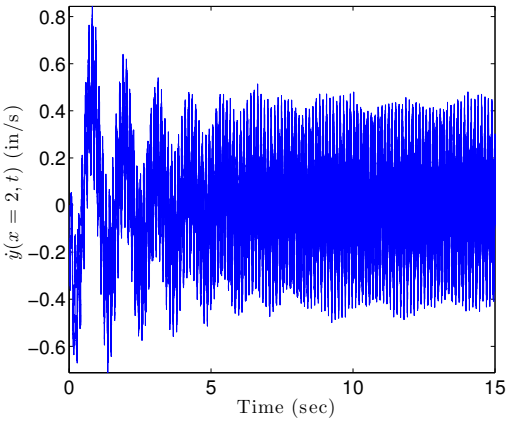

Figure 20. $\dot{y}(x = 2, t)$ **Designed Gains**

V. Discussion & Conclusion

The generalized state space approach provided closed form solution for the system frequency response for both the tip mass and the no tip mass models. Several other boundary conditions can be applied and the same steps presented here can be followed in order to obtain the analytical solutions. By utilizing the full transfer function solution provided by the GSS approach any control problem design in the frequency domain can be addressed. A case study is constructed for the gain selection of a Lyapunov stable control law. By looking at the frequency response and changing the gains an acceptable performance was achieved driving the structure from a stationary initial state to a target state while suppressing the beam vibrations. The examined control law with the selected gains was not able to fully suppress the appendage vibrations while driving the rigid hub to the desired state. This can be mitigated by constructing a closed loop control following a given reference trajectory or by applying notch compensation to the control law to suppress undesirable vibrations.

The presented control problem has potential for several extensions. Optimization was not considered in this work whereas several techniques exists for optimization in the frequency domain based Parseval's theorem. In general the GSS provides a general test bed for any control scheme in the frequency domain. This is a very powerful tool as it avoids relying on approximate models and truncated series.

References

[1] Lupi, V., Turner, J., and Chun, H., "Transform Methods for Precision Continuum and Control Models of Flexible Space Structures," *Proceedings of the AIAA/AAS ASTRODYNAMICS Conference*, Portland, Oregon, August 20-22 1990, pp. 680 – 689.

[2] Lupi, V., Chun, H., and Turner, J., "Distributed Modeling and Control of Flexible Structures," *Presented at the IFAC Workshop in Dynamics and control of Flexible Aerospace Structures: Modeling and Experimental Verification*, Huntsville, Alabama, April 2 –4 1991.

[3] Lupi, V., Chun, H., and Turner, J., "Distributed Control and Simulation of a Bernoulli-Euler Beam," *Journal of Guidance, Control and Dynamics*, Vol. 15, No. 3, 1992, pp. 729 – 734.

[4] Meirovitch, L. and Quinn, R., "Equations of motion for maneuvering flexible spacecraft," *Journal of Guidance, Control, and Dynamics*, Vol. 10, No. 5, 1987.

[5] Meirovitch, L. and Stemple, T., "Hybrid equations of motion for flexible multibody systems using quasicoordinates," *Journal of Guidance, Control, and Dynamics*, Vol. 18, No. 4, 1995.

[6] Junkins, J. L. and Kim, Y., *Introduction to dynamics and control of flexible structures*, AIAA, 1993.

[7] Lee, S. and Junkins, J., "Explicit Generalizations of Lagranges' Equations for Hybrid Coordinate dynamical Systems," *Journal of Guidance, Control and Dynamics*, Vol. 15, No. 6, 1992, pp. 1443 – 1452.

[8] Junkins, J. and Turner, J., *Optimal Spacecraft Rotational Maneuvers, studies in Astronautics*, Elsevier Scientific Publishing company, New York, NY, 1985.

[9] Turner, J. and Junkins, J., "Optimal large-angle single-axis rotational maneuvers of flexible spacecraft," *Journal of Guidance, Control, and Dynamics*, Vol. 3, No. 6, 1980.

[10] Turner, J. and Chun, H., "Optimal distributed control of a flexible spacecraft during a large-angle maneuver," *Journal of Guidance, Control, and Dynamics*, Vol. 7, No. 3, 1984, pp. 257 – 264.

[11] Wie, B., Sinha, R., and Liu, Q., "Robust time-optimal control of uncertain structural dynamic systems," *Journal of Guidance, Control, and Dynamics*, Vol. 16, No. 5, 1993.

[12] Boškovic, J., Li, S., and Mehra, R., "Robust adaptive variable structure control of spacecraft under control input saturation," *Journal of Guidance, Control, and Dynamics*, Vol. 24, No. 1, 2001.

[13] Turner, J. D. and Elgohary, T. A., "Generalized Frequency Domain State-Space Models for Analyzing Flexible Rotating Spacecraft," *Advances in Astronautical Science: The Kyle T. Alfriend Astrodynamics Symposium*, Vol. 139, 2011, pp. 483 – 500.

[14] Elgohary, T. A. and Turner, J. D., "Generalized Frequency Domain Modeling and Analysis For A Flexible Rotating Spacecraft," *AIAA Modeling and Simulation Technologies (MST) Conference*, AIAA, Boston, MA, August 19 – 22 2013.

[15] Turner, J. D. and Elgohary, T. A., "Generalized Frequency Domain State-Space Models for Analyzing Flexible Rotating Spacecraft," *The Journal of the Astronautical Sciences*, Vol. 59, No. 1-2, 2014, pp. 459–476.

[16] HALE, A. L., Lisowski, R. J., and DAHL, W. E., "Optimal simultaneous structural and control design of maneuvering flexible spacecraft," *Journal of Guidance, Control, and Dynamics*, Vol. 8, No. 1, 1985.

[17] Maganti, G. B. and Singh, S. N., "Simplified adaptive control of an orbiting flexible spacecraft," *Acta Astronautica*, Vol. 61, No. 7, 2007, pp. 575 – 589.

[18] Junkins, J., Rahman, Z., and Bang, H., "Near-minimum-time control of distributed parameter systems-Analytical and experimental results," *Journal of Guidance, Control, and Dynamics*, Vol. 14, No. 2, 1991.

[19] Breakwell, J., "Optimal feedback slewing of flexible spacecraft," *Journal of Guidance, Control, and Dynamics*, Vol. 4, No. 5, 1981.

[20] Ben-Asher, J., Burns, J., and Cliff, E., "Time-optimal slewing of flexible spacecraft," *Journal of guidance, control, and dynamics*, Vol. 15, No. 2, 1992.

[21] Singh, G., Kabamba, P., and McClamroch, N., "Planar, time-optimal, rest-to-rest slewing maneuvers of flexible spacecraft," *Journal of Guidance, Control, and Dynamics*, Vol. 12, No. 1, 1989.

[22] Dwivedy, S. and Eberhard, P., "Dynamic analysis of flexible manipulators, a literature review," *Mechanism and Machine Theory*, Vol. 41, No. 7, 2006, pp. 749–777.